Observation of soil behavior during pressing pile: Considering the effect of multiple layer and particle size

N. Suzuki, N. Ogawa, Y. Ishihara
GIKEN LTD. , Tokyo, Japan
K. Nagai
Professor, Graduate School of Engineering, Hokkaido University, Sapporo, Japan

ABSTRACT

When piles are installed near existing structures, there is concern about their impact on the underground structure. This study adopts a model test and numerical analysis to observe soil behavior during the pile installation, focusing on multiple layers and particle size, whose effects are difficult to observe in limited-size model tests. First, we developed a system to measure soil deformation during the installation of a pile, using inclinometers. 1g model tests were conducted to simulate the pile installation into the sand and gravel layers and measure penetration resistance, earth pressure, and soil deformation. Second, the 2D Rigid Body Spring Model (RBSM), one of the discrete and static analysis methods, was used to consider the influence of particle size and pile diameter on soil deformation. In both methods, it was observed that larger particles transmitted forces to a deeper location and increased the displacement variation (i.e., maximum displacement), which is presumably due to the mechanism of the granular material.

Keywords: *Soil deformation, Inclinometer, Multi-layer ground, 1g model test, Discrete analysis*

1. Introduction

When piles are installed near existing structures, there is concern about their impact on underground structures such as power lines and water supply facilities (Nagai et al., 2018).

Various techniques have been applied to observe soil deformation during pile penetration in model tests, such as colored sands (Horii et al., 2007), aluminum rod–laminate ground, X-ray CT (Otani et al., 2003), photoelastic material (Dijkstra et al., 2011), etc. Colored sands are limited to two-dimensional observation, and the other complex techniques limit the size of the test specimen. Such limited-size tests make it difficult to observe the effects of pile penetration, especially in middle or complex soil layers with granular materials such as cobbles. A measuring device large enough to observe soil deformation from the beginning to the end of pile penetration is required.

This paper aims to develop such a measurement device and explore the influence of particle size on soil deformations during pile penetration. Soil deformations are observed during pile penetration using inclinometer sensors, which have been used primarily for slope collapse measurements (Uchimura et al., 2010), with the anticipation of future on-site measurements. 1g model tests are conducted, taking pile diameter and soil type as parameters. Additionally, a discrete analysis called 2D-RBSM (two-dimensional rigid body spring model) is conducted to check the validity of the model tests.

2. Experimental method

2.1 Overview and measurements

Fig. 1 shows the experimental apparatus. The front and back of the soil tank were made of acrylic plates and the sides were made of iron plates, with a height of 1700 mm and width and length of 1000 mm (Ogawa et al., 2011).

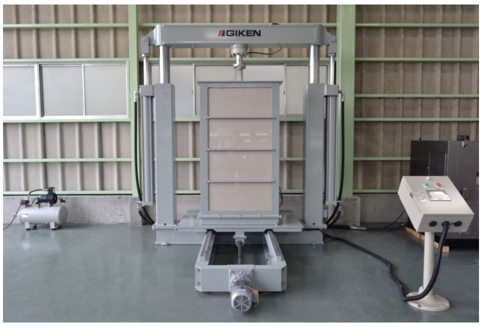

Fig. 1 Overall view of the test apparatus

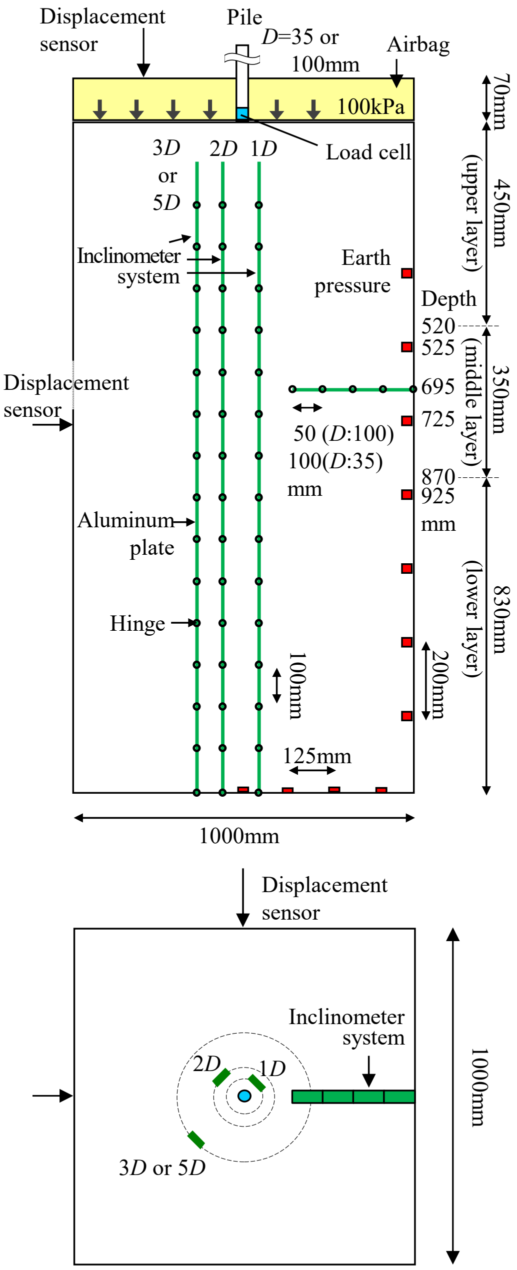

Fig. 2 Position of measurement devices. *D* is pile diameter.

After installing the inclinometer sensors, the soil tank was filled with dry sand using the free-fall method. A closed-ended steel pipe pile (STKM12B, JISG3445), 35 or 100 mm in diameter and 1200 mm in length, was pressed in through the center of the tank.

During pile penetration, penetration resistance, tip resistance, soil displacement, earth pressure, and wall displacement were measured. **Fig. 2** shows the position of the measurement devices.

Soil deformation was observed through inclinometer systems. Horizontal displacement was obtained by three systems and vertical displacement was obtained by one system in the middle layer.

Seven earth pressure gauges were installed on the left side, and four on the bottom. Displacements of the soil tank were measured at the top and the side by rod-type displacement sensors.

2.2 Inclinometer system

Fig. 3 shows the concept of obtaining displacements by inclinometers. After inclinometer measure rotation θ, displacements at each hinge were calculated by accumulating displacements from the point pinned to the bottom/side of the soil tank.

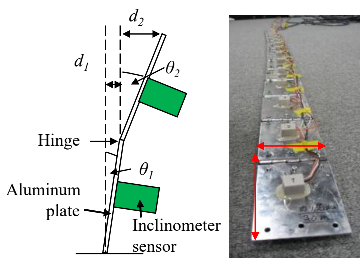

Fig. 3 Concept of displacement measurement by inclinometers

Four aluminum plates were attached to the inclinometer to obtain vertical displacement and 15 plates were attached to the inclinometer to obtain horizontal displacement. The width of the plate was 35 mm, and the length was 50 mm only for those obtaining the vertical displacement with a pile diameter of 100 mm, while the length was 100 mm for all others. The length of each hinge joint was 5 mm.

2.3 Experimental Procedure

To transmit a surcharge deeply, Teflon sheets were attached to the walls of the emptied soil tank. The vertical inclinometer measurement systems were pinned at the lower end of the soil tank and strapped to a rod temporarily passed through the top of the tank (**Fig. 4**).

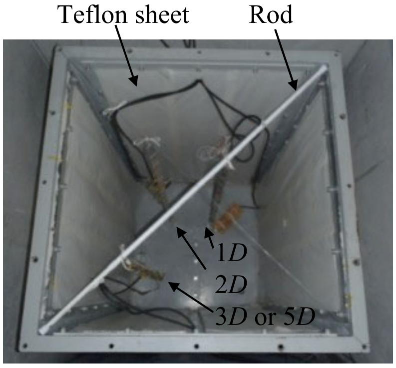

Fig. 4 Installation of inclinometer system

The model ground was made by the free fall of dry sand, while the verticality of the inclinometer was visually checked. The sand fell from a 600 mm height from the ground surface, and when the ground surface was more than 500 mm below the soil tank top, the sand fell from the soil tank top.

In the multi-layer test case, the middle layer, to a depth of 520-870 mm, consisted of gravels (crushed stones). Gravels were placed manually, dropping wooden sticks at every 10 mm and compacting them.

The inclinometer system was installed at a depth of 695 mm from the soil tank top. When the sand was filled, the inclinometer fixings were removed from the rods, the sand was sucked out with a vacuum cleaner, and the ground surface was leveled.

Airbags and a soil tank cover were installed, and a surcharge of 100 kPa was applied by air. After the earth pressure on the tank wall was stabilized, the values of the inclinometers were initialized. The pile penetrated at a rate of 20 mm/sec and terminated at a depth of 1000 mm where the influence of the bottom boundary was negligible.

2.4 Test Cases

Table 1 lists test cases. Four cases were tested, including a single-layer series using silica sand and a multi-layer series using gravel, positioned in the middle of the soil layer.

Table 2 lists the properties of silica sand (No. 6) and gravel (crushed stones, No. 7). The relative density ranged from 55 to 70% for the sand layer and 100% for the gravel layer. The silica sand-steel friction coefficient was estimated to be 0.4 from a simple test examining the ratio of bearing load to sliding onset load, which closely matched the well-known formula $\tan(2/3\phi)$, where internal friction angle of the sand ϕ was 35 degrees.

Table 1 Model test cases

Case	Layer type	Pile diameter D, [mm]	Distance from inclinometer system to pile surface
S-35	Single	35	1D, 2D, 5D
S-100	Single	100	1D, 2D, 3D
M-35	Multi	35	1D, 2D, 5D
M-100	Multi	100	1D, 2D, 3D

Table 2 Soil properties

	Minimum density [g/cm^3]	Maximum density [g/cm^3]	Particle density [g/cm^3]	Particle size d_{50} [mm]
Silica sand	1.24	1.52	2.65	0.18
Gravel	1.43	1.60	-	3.2

3. Experimental results

3.1 Penetration resistance

Fig. 5 shows the changes in unit tip resistance. Unit tip resistance in Cases S-35/100 stabilized at 3 MPa from a certain depth, and little difference was observed by pile diameter. Unit tip resistance in Cases M-35/100 increased from before the gravel layer, reaching a peak of 7 MPa within the gravel layer. Subsequently, the unit tip resistance gradually decreased before penetration into the lower layer. Unit tip resistance increased from 2.5D or more before entering the middle layer and decreased from 2.5D before leaving the middle layer, which is consistent with previous studies (Horii et al., 2007).

After some penetration, the shaft resistance was 25% of the penetration resistance for S/M-35 cases and 10% for S/M-100 cases.

3.2 Lateral Earth Pressure

Fig. 6 illustrates the changes in lateral earth pressure installed around the middle layer. In cases of the single layer, the lateral pressure peaked at a depth almost identical to the pile tip. On the other hand, in cases of the

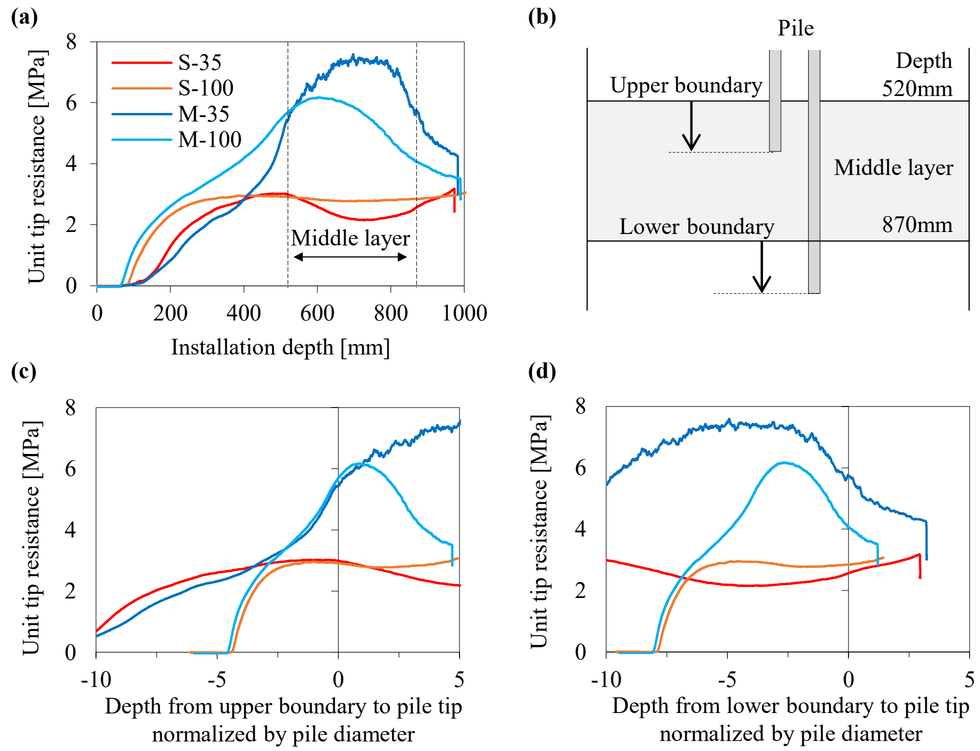

Fig. 5 Unit tip resistance during pile penetration. (a) tip resistance is divided by the area of the pile tip. (b) explaining depth from the upper/lower boundary of the middle layer to the pile tip, which are the axes of the figures (c) and (d).

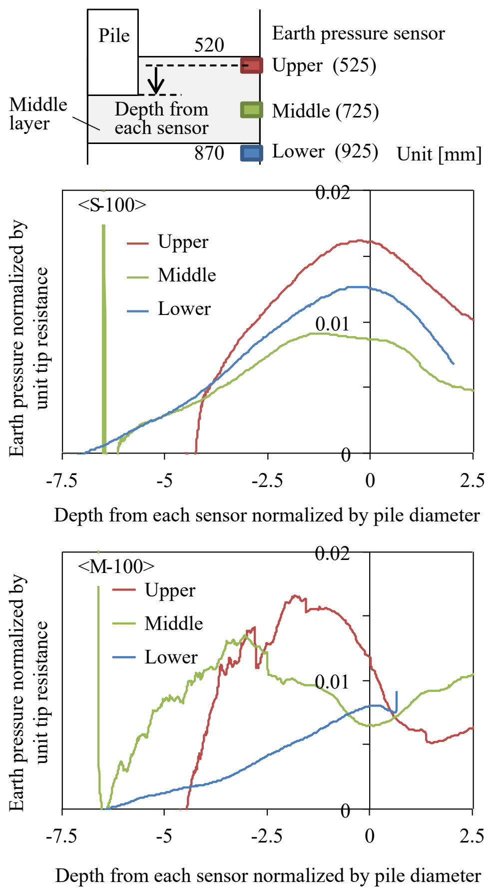

Fig. 6 Change in earth pressure during pile penetration

multi-layer, the lateral pressure in the middle layer (green line) reached a peak earlier than the others, while the maximum values were almost the same.

This implies that the stress transmission in the ground due to pile penetration depends on the soil type, especially in gravel layers, where stress can be transmitted deeply.

It is to be noted that in Cases S/M-35, it was not possible to measure a stable soil pressure increment because the soil pressure sensor was relatively far away and the increase in earth pressure was less than in Cases S/M-100.

3.3 Soil deformation

Fig. 7 depicts soil deformation measured by the inclinometer systems. The plates laterally moved up to approximately 10 mm from the initial state.

With penetration, horizontal displacement peaked at the depth of the pile tip, and deformation spread downward. As the pile diameter increased, the deformation spread deeper into the ground.

Fig. 8 shows the change in lateral displacement at a depth of 750 mm, which is in the middle layer (520-870

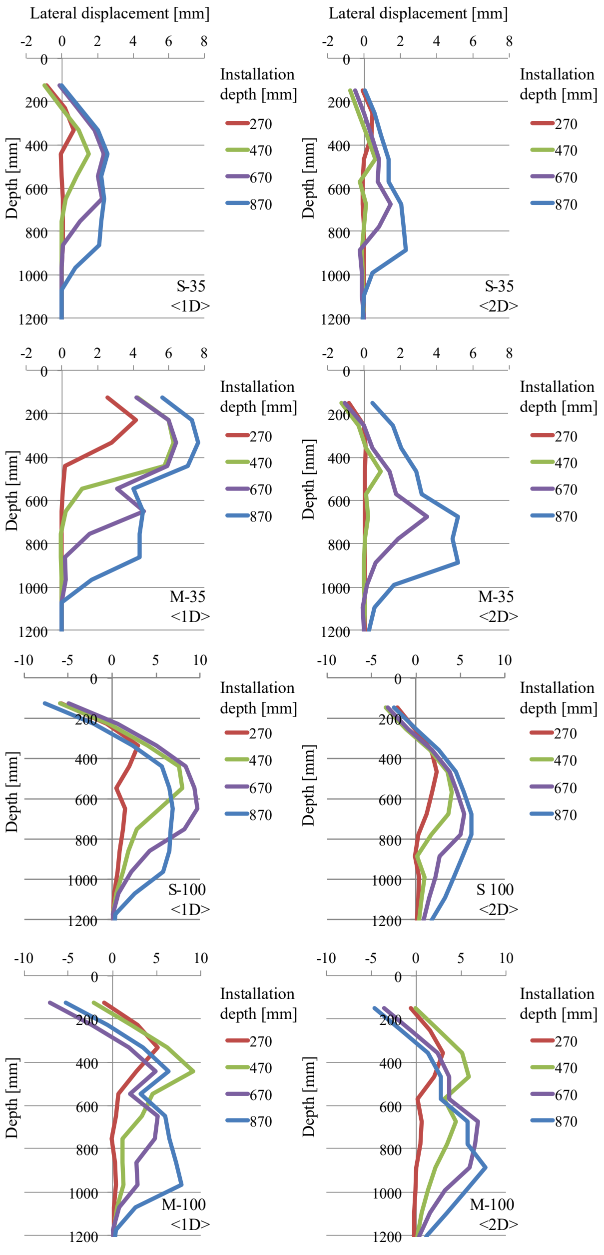

Fig. 7 Soil deformation during pile installation

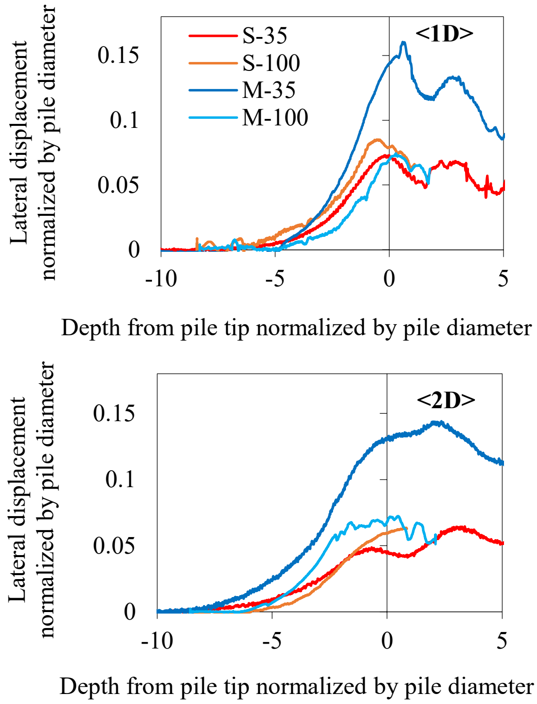

Fig. 8 Change in lateral displacement during pile penetration at 750 mm depth.

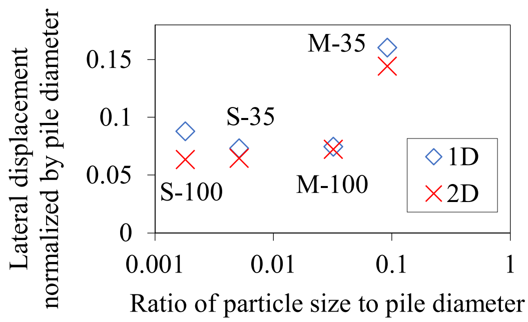

Fig. 9 Relationship between maximum lateral displacement and ratio of particle size to pile diameter at 1*D* and 2*D*

mm), during pile penetration. In all cases, lateral displacements started around 6*D* to 8*D* below the pile tip, reaching a peak when the pile tip reached the same depth.

Lateral displacements decreased in 1*D* after the peak, while in 2*D*, they remained constant. This suggests that, near 1*D*, deformations occur in the direction approaching the pile surface after the pile tip passes through at 1*D*. However, in Case M-35, both 1*D* and 2*D* showed larger displacement than in other cases.

Fig. 9 shows the relationship between the ratio of particle size to pile diameter and maximum lateral displacement at a depth of 750 mm.

Clearly, only Case M-35 showed significant horizontal displacement. Since this was attributed to the effect of the particle size, a detailed study will be conducted in the next section by numerical analysis to exclude experimental errors and differences in relative density.

4. Numerical Simulation

4.1 Analysis Method

The rigid body spring model (RBSM; Kawai, 1978) reproduces the subject of analysis using discrete rigid body elements and calculates stress transmission between elements using springs placed between them. In RBSM, unlike Discrete Element Method (DEM), the equilibrium of forces among elements is assumed, rather than calculated through motion equations.

In this study, a 2D program based on the RBSM developed for concrete fracture analysis was used, with modifications to accommodate large deformation behavior (Nagai et al., 2011). The program performs contact detection at each step, placing springs between elements if their distance is less than specified and removing springs if the distance exceeds the threshold (**Fig. 10**).

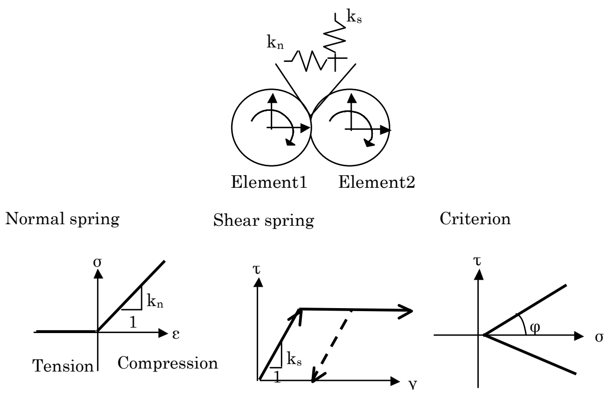

Fig. 10 Circular element and spring, and constitutive equation

Table 3 lists the parameters used in RBSM, which were determined to be qualitatively similar to the results of direct shear tests with Toyoura sand (Nagai et al., 2011). Note that the difference in element density from that of the actual sand is due to the difference in packing efficiency in 2D and 3D.

The analysis comprised the following steps:

- randomly placing circular elements simulating sand in a rectangular container. Particle size ranged from 4.8 to 7.2 mm, with an average of 6.0 mm, d_{50}.
- free falling the elements and flattening the surface.
- applying an overburden pressure using larger elements (particle size: 10 mm, gravity constant 1000 times). The pressure was maintained during pile installation.
- reducing the friction temporarily to make the void ratio approximately 0.20.
- pressing a pile (rectangular element) by 0.25 mm per step.

Due to memory limitations in cases with numerous elements, a symmetry assumption was made (**Fig. 11**b). **Table 4** lists the analysis case. The size of the soil tank was adjusted to run the program. The particles were the same size, while the width of the pile D and the size of the tank were different in the cases.

Cases marked with * in **Table 4** were conducted to examine the effect of tank width and pile type on the results. Since there was little difference in resistance in each case, it was determined that there was little effect observed; this was omitted in this paper due to space constraints.

Table 3 Parameters used in RBSM

Item			Unit
Elastic modulus, E		75	MPa
Shear stiffness, G		5	MPa
Friction angle φ between	Sand-sand	30	degrees
	Sand-wall	10	degrees
	Sand-pile	0	degrees
Step displacement of the pile		0.25	mm
Element density		2.0	g/cm^3
Poisson's ratio		0.3	

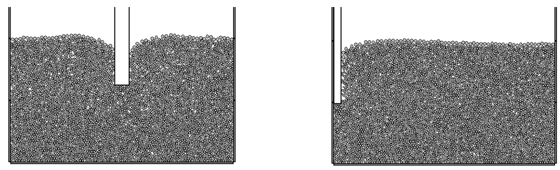

(a) full (b) half

Fig. 11 Analysis image

Table 4 Analysis of cases and conditions

Case	Pile		Soil tank		Ratio	
	Type	Width D [mm]	Width [mm]	Depth [mm]	d_{50}/D	Tank width/D
case1-1	full	10	600	330	0.6	60
case1-2*			300	330		30
case2-1	full	20	600	330	0.3	30
case2-2*			300	330		15
case3-1	full	40	600	600	0.15	15
case3-2*	half		600	600		30
case4	half	80	600	600	0.075	15
case5	half	120	600	600	0.05	10

Notes: * represents comparison test case to check the effect of boundary and pile type. d_{50} is the mean particle size.

4.2 Simulation results

Fig. 12 shows the analysis results of cases with d_{50}/D of 0.075 and 0.3. Normal stress transmitted by particle contact is expressed by red lines. Larger particles reduced the number of red lines and limited the number of particles transmitting normal stress. The diagram of maximum shear strain shows a cone under the pile tip and Meyerhof rupture surface. The horizontal displacement diagram demonstrates deformation symmetrically centered on the pile. Larger particles caused deeper deformation. The maximum lateral displacement occurred slightly away from the pile center.

Fig. 13 shows the relationship between particle size and lateral displacement, focusing on position 1*D* away from the pile surface (i.e., 1.5*D* from the pile center). As the particle size increased, both the variability and average displacement increased, which is consistent with the trends observed in the model experiments (**Fig. 9**). Notably, the ratio of particle size to pile width differed between model tests and numerical analysis.

Given the variation in the displacement measured in the numerical analysis, the displacement measured in the model test could represent a local maximum. The increase in variability can be attributed to asymmetric soil deformations occurring vis-a-vis the pile center during pile penetration. Nagai et al. (2011) attempted to apply the buckling theory to the process of pile penetration into granular materials and explained particle contact/slip on the micro-scale, buckling of a series of particles on the mesoscale, and shear phenomena on the macro scale. (**Fig. 14**). This granular connection could transfer forces to deeper locations and increase the variations (i.e., the maximum) in displacement.

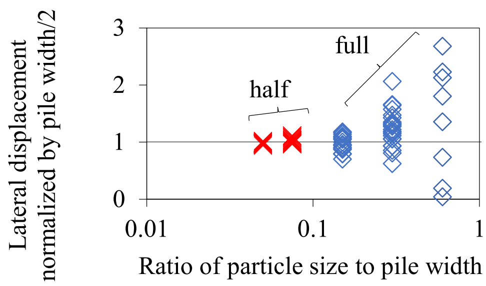

Fig. 13 Relationship between lateral displacement and the ratio of particle size to pile width (d_{50}/D) at 1*D* from pile surface. "full" and "half" are type of the pile. Displacements were normalized not by the pile width, but the half, so that the value would be 1 if the volume of the penetrated pile matched the volume of the displaced sand.

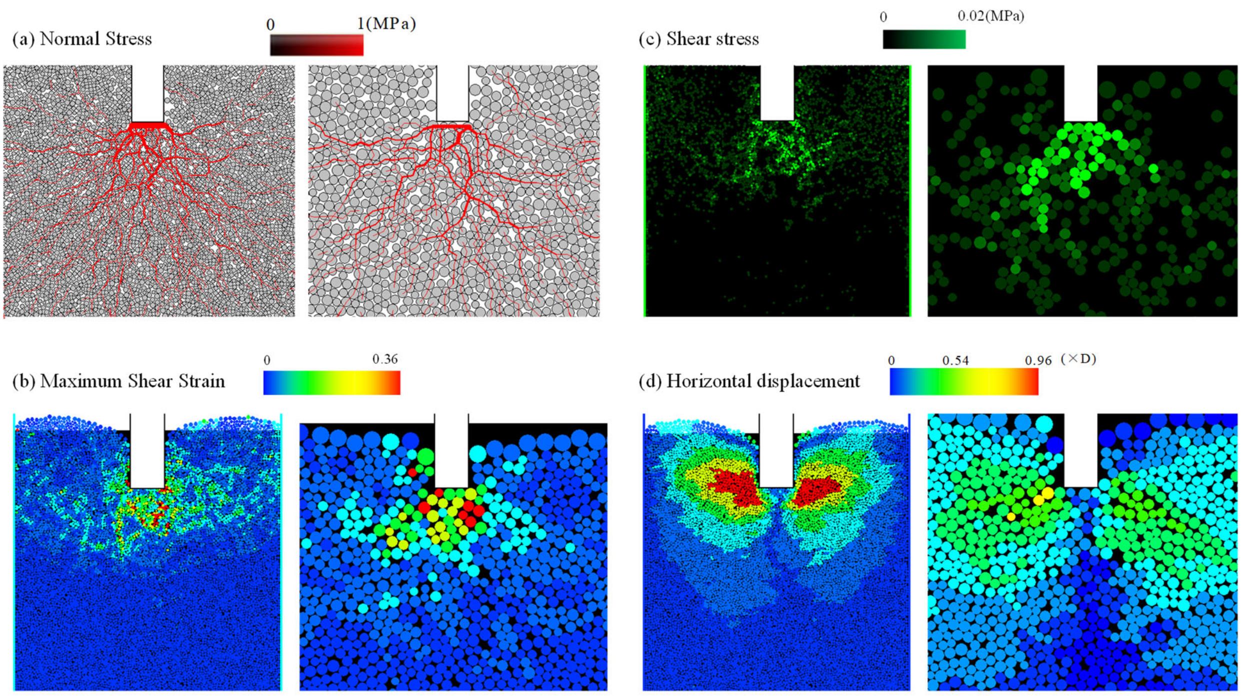

Fig. 12 Analyses results. d_{50}/D=0.075 and 0.3. a) Normal stress, b) maximum shear strain, c) shear stress, d) horizontal displacement.

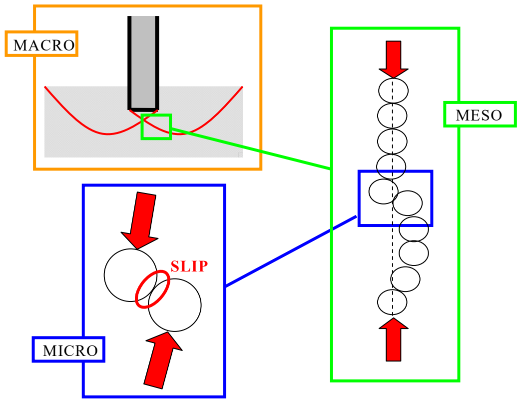

Fig. 14 Mechanism of structural collapse of granular materials in piles (Nagai et al., 2011).

5. Summary

This study conducted 1g model tests and 2D numerical analysis to observe the soil deformation during pile penetration, considering the effect of the particle size and multi-layers. The following results were derived from the model tests:

- Unit tip resistance increased/decreased from 2.5*D* before entering/exiting the gravel layer, with little difference due to pile diameter.
- The horizontal earth pressure during pile penetration peaked at the same or deeper depth as the pile tip in the sand layer and was transmitted to a greater depth in the gravel layer.
- Horizontal displacement was proportional to the pile diameter in the single-layer case. This was also true of the multi-layer case with a large diameter pile, whereas that with a small diameter pile was about twice as large. This would be the effect of the particle size divided by the pile diameter.

Similar results were derived from the 2D numerical analysis, although simple comparisons were difficult. Especially in the case of large particles, the scatter in the analysis results was large. From a research perspective, this will require a probability-based analysis.

Importantly, the ratio of particle size to pile diameter had little effect on the tip resistance, whereas it had a significant effect on the soil deformation. Thus, observing the tip resistance alone is not sufficient to understand soil behavior. From a practical point of view, preliminary investigation or on-site observation are necessary, if large-size sands/stones are foreseeable,

References

Dijkstra, J., Alderlieste, E., Broere, W., van Tol, A., 2011. Experimental investigation into the stress and strain development in a open ended tubular pile. In: Proceedings of 3rd IPA International Workshop in Shanghai. IPA, pp. 46–54.

Horii, Y., Watanabe, T., Nagao, T., 2007. Study on Vertical Bearing Properties of Intermediate-Layer-Supported Piles: Centrifuge Model Tests with Intermediate-Layer Thickness as a Parameter. TAISEI Tech. Cent. Rep. 40, 6p. (in Japanese)

Kawai, T., 1978. New discrete models and their application to seismic response analysis of structures. Nucl. Eng. Des. 48, pp. 207–229.

Nagai, K., Suzuki, N., Ishihara, Y., Uchimura, T., 2018. An Investigation of Effect of Distance and Shape of Pile on the Displacement of Gag Pile by 3D FEM Analysis. In: The 1st International Conference on Press-in Engineering 2018, Kochi. IPA, pp. 429–434.

Nagai, K., Uchimura, T., Sakai, Y., Maekawa, K., 2011. Numerical simulation of press-in behavior in a heterogeneous field using aluminum rods layer by discrete analysis method. In: Proceedings of 3rd IPA International Workshop in Shanghai. IPA, Shanghai, pp. 32–45.

Ogawa, N., Yamane, T., Ishihara, Y., Shiraishi, T., Nagai, K., 2011. Basic experiment of press-in piling using model ground: Outline of experimental apparatus and procedure for making model ground. In: Proceedings of Japan Society of Civil Engineers, Shikoku Branch Technical Research and Presentation Vol: 17. pp. 149-150 (III–16). (in Japanese)

Otani, J., Hironaka, J., Mukunoki, T., 2003. Visualization of failure patterns under vertically loaded pile foundation using X-ray CT method. In: Proc. 12th Asian Regional Conference on Soil Mechanics and Geotechnical Engineering. pp. 973–976.

Uchimura, T., Towhata, I., Anh, T.T.L., Fukuda, J., Bautista, C.J.B., Wang, L., Seko, I., Uchida, T., Matsuoka, A., Ito, Y., Onda, Y., Iwagami, S., Kim, M.S., Sakai, N., 2010. Simple monitoring method for precaution of landslides watching tilting and water contents on slopes surface. Landslides 7.